Direct Bilirubin Detection Using Surface-Enhanced Raman Spectroscopy

Cheng-Yi Li, Sandy Huey-Jen Hsu, Cheng-Chung Chang**, and Gou-Jen Wang*

***Abstract*—Biliary atresia is the most common cause of childhood liver disease and is the main cause of liver replacement. The use of an effective early screening technique can efficiently improve the therapeutic effect on children with biliary atresia, especially those in the remote rural areas. This study introduces a novel method for detecting direct bilirubin by Raman spectroscopy using composite surface-enhanced Raman spectroscopy (SERS) chips. These chips were created by spreading silver nanowires on the nanostructure surface of an anodic aluminum oxide substrate. Experimental results demonstrated that the detection limit of direct bilirubin concentration vastly improved far below the disease criteria of bilirubin in adults and infants. Meanwhile, using only 10 μL of direct bilirubin, a wide detection range from 10^{-7} to 10^{-4} M was obtained, covering the clinic reference range with R^2 of 0.98336 at the peak value of 1.616 cm^{-1}. Furthermore, the results revealed that the proposed composite SERS substrates possessed good statistical relative standard deviation and reproducibility (N = 3) of 4.6% and 2.2%, respectively. Thus, the composite SERS chip combined with the Raman spectroscopy approach can be integrated with portable Raman spectrometer for the effective clinical detection of direct bilirubin.**

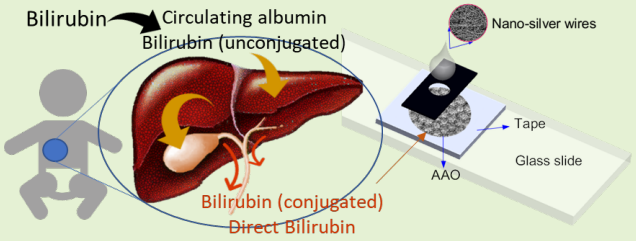

***Index Terms*—direct bilirubin detection, surface-enhanced Raman spectroscopy, composite SERS substrate**

I. Introduction

BILIARY atresia, a congenital disease, is the most common cause of childhood liver disease and is the main cause of liver replacement [1]. This disease is characterized by the partial or total occlusion of the extrahepatic bile duct system, thus leading to cholestasis and biliary cirrhosis. If treatment is delayed, patients may eventually die of liver failure resulting from liver cirrhosis [2]. The three main clinical signs of biliary atresia are gray stools, delayed jaundice, and brown urine. These clinical manifestations can be observed in infants to determine whether there is a possibility of bile retention [3]. At present, surgery (Kasai surgery) is the main treatment option for biliary atresia. Better cure rates among patients can be achieved with the timely detection of biliary atresia and the immediate performance of Kasai operation [4]. Therefore, the development of early screening and early diagnosis technologies is instrumental in effectively improving the therapeutic effects on children with biliary atresia. Harpavat et al. pointed out that direct bilirubin concentrations in infants with biliary atresia increase soon after birth; thus, direct bilirubin can be used as a critical indicator for screening biliary atresia. Specifically, if infants have direct bilirubin levels exceeding 5.1 μM or if direct bilirubin accounts for over 20% of the total bilirubin detected, then they are considered biliary atresia patients [5].

Bilirubin is the main metabolite of heme; its normal daily output of approximately 300 mg [6, 7] is considered toxic and can cause damage to the nervous system. In the body, bilirubin is mainly derived from the disintegration of aging red blood cells. In particular, heme is catalyzed by hemooxygenase to form biliverdin, which is then reduced to bilirubin by biliverdin reductase. Bilirubin in the body can be divided into two types: conjugated and unconjugated bilirubin. Conjugated bilirubin, also known as direct bilirubin, can react quickly with diazo reagents. Unconjugated bilirubin, also called indirect bilirubin, contains hydrogen bonds and reacts slowly with diazo reagents. Unconjugated bilirubin is fat-soluble and toxic, and most of it is transported to the liver for metabolism by binding to albumin in the blood. At the same time, unconjugated bilirubin may interact with glucuronic acid in the liver to form water-soluble and less toxic conjugated bilirubin. The conjugated bilirubin, now in the form of bile, is finally discharged into the intestine through the biliary tract. To complete the metabolic process of bilirubin in the body, most of it is excreted with feces, and a small part is excreted with urine [8, 9]. Bilirubin metabolism is closely related to hepatobiliary function; thus, the concentration of bilirubin in the body can be used as an indicator of hepatobiliary diseases. For instance, a high level of indirect bilirubin concentration may be caused by the

This work was supported by the Ministry of Science and Technology of Taiwan (grant # MOST-108-2622-E-005-017-CC2). Cheng-Yi Li is with the Department of Mechanical Engineering at the National Chung-Hsing University, Taichung 40227, Taiwan.

Sandy Huey-Jen Hsu is with the Department of Laboratory Medicine, National Taiwan University Hospital, Taipei 10002, Taiwan.

Cheng-Chung Chang** is with the Graduate Institute of Biomedical Engineering at the National Chung-Hsing University, Taichung 40227, Taiwan. (email: ccchang555@dragon.nchu.edu.tw)

Gou-Jen Wang* is with the Department of Mechanical Engineering & the Graduate Institute of Biomedical Engineering at the National Chung-Hsing University, Taichung 40227, Taiwan. (email: gjwang@dragon.nchu.edu.tw)

destruction of liver cells, which degrades the body's ability to convert and excrete bilirubin. If the direct bilirubin concentration is too high, this may be caused by biliary obstruction [10]. The normal levels of total, conjugated, and unconjugated bilirubin in the serum of healthy people range from 5.1–17.0, 1.0–5.1, and 1.7–10.2 μM, respectively [9]. Many methods have been developed for bilirubin detection, such as the diazo method, high performance liquid chromatography (HPLC), spectrophotometry, electrochemical method, fluorometry, and surface-enhanced Raman spectroscopy (SERS) [11, 12].

Bilirubin can be coupled with diazonium ions to form colored azo compounds through diazo reaction. After the reaction, the color of the reagent is proportional to the concentration of bilirubin, hence the diazo method is widely used for quantitative determination of serum bilirubin. However, the diazo reagent is unstable and must be synthesized from sodium nitrite and aminobenzenesulfonic acid, and is easily affected by pH [13]. The standard method for measuring bilirubin in serum samples is HPLC, because of its advantages of non-interference with other heme proteins [14] and its ability to quickly and sensitively separate and detect direct and indirect bilirubin. The disadvantage is that the instrument is expensive and requires the service of professionals to perform the procedure. Electrochemical bilirubin detection can be divided into enzyme and enzyme-free methods. On the basis of the co-catalysis of bilirubin oxidase box and graphite oxide nanoparticles Chauhan et al. proposed an electrochemical enzyme sensor that has a detection limit of 0.1 nM and a linear range of 0.01–500 mM [15]. Estimating bilirubin in infant serum using spectrophotometry is a simple and fast method. However, this method is only applicable to infants under 2–3 weeks of age; given that older infants could ingest substances with lower absorption wavelengths, such as carotenoids, this can affect the accuracy of spectrophotometry [16]. Fluorometry is divided into enzyme and non-enzyme methods. Changes in fluorescence depend on the concentration and type of bilirubin; hence, direct and indirect bilirubin concentrations can be estimated by the difference in fluorescence/absorption values before and after the reaction [17, 18]. Santhosh et al. proposed an enzyme-free method based on fluorescence quenching. Using gold nanoclusters that are stabilized to human serum albumin as fluorescent probes is a sensitive and reliable way of detecting bilirubin concentrations in serum [19]. Although the fluorescence method can sensitively detect the concentration of bilirubin, it is susceptible to environmental factors, such as pH and temperature. Meanwhile, SERS is a label-free detection technology that can directly provide the intrinsic SERS signal of the biomarker of interest in complex biological matrices and can be used without the need to label action or special treatment on the SERS substrate and samples [20]. Pan et al. presented an accurate method of diagnosing jaundice and related diseases by proposing a paper-based SERS biosensor for the label-free and sensitive detection of bilirubin concentration in serum [21].

The current study proposes a novel method for detecting direct bilirubin by Raman spectroscopy. The main feature of this method is the use of the composite SERS chip, which combines silver nanowires (SNWs) and a silver thin film-coated anodic aluminum oxide (AAO) substrate to achieve the double enhancement of surface Plasmon resonance (SPR), thereby enhancing the detection limit of direct bilirubin. First, the nanostructure platform was constructed, after which the optimized plasma-enhance effect was explored based on the ratio between the SNW and AAO substrate. Eventually, the nanoplatform was successfully applied to detect the direct bilirubin and determine the detection limit. Evaluating the future application and development of this platform can be further investigated in the future. Meanwhile, the composite SERS substrate can be further integrated with portable Raman spectrometer for direct bilirubin detection. This way, we can quickly and effectively detect whether a newborn is suffering from biliary atresia.

II. Materials and Methods

A. Preparation of the Composite SERS Chips

The schematic of the proposed composite SERS chip is shown in Figure 1. First, the composite SERS chip was fabricated by depositing SNWs on a silver thin film-coated AAO membrane, which was prepared by coating a silver thin film on a surface-modified AAO membrane with a barrier-layer surface modification substrate. The void space enclosed by the tape served as the well to hold the target sample.

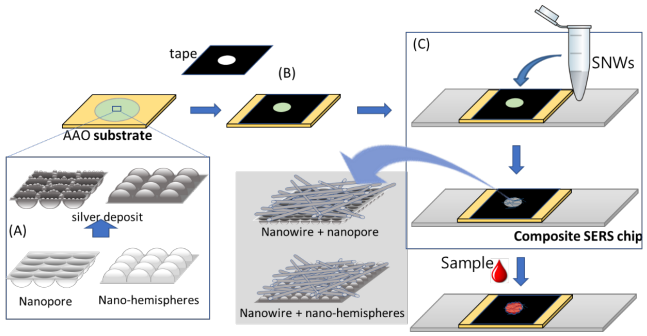

Fig 1. Schematic of the proposed composite SERS chip and the sample detection. (A) silver thin film coating on AAO membranes; (B) SERS chip packaging; (C) SNW deposited on the silver thin film-coated AAO membrane

1) *SNW preparation*

The polyol method was used for the preparation of SNWs [22]. At a stirring speed of 600 rpm, 60 mL of ethylene glycol was heated to 170 °C. Once the temperature stabilized for 5 min, 300 μL of 3.2 mM NaCl was added into the system and heated for 18 min. Then, 20 mL of 0.150 M polyvinylpyrrolidone (PVP) was added into the system. After 12 min, 20 mL of 0.186 M $AgNO_3$ was added, and the solution was heated and stirred continuously for 120 min to obtain the SNW solution (Optical density, OD = 1).

2) *AAO substrate preparation*

(1) *AAO film preparation*

The well-known anodizing process was employed for the preparation of the AAO membranes. Aluminum foils were cleansed and electropolished before anodization. The anodizing process was conducted by placing the electropolished aluminum foil in a 0.3 M phosphoric acid solution under an applied voltage of 50 V at –2.5 °C for 5.5 hours. The non-oxidized aluminum beneath the barrier layer was then

removed using an HCl aqueous containing 1 M $CuCl_2$ to obtain a honeycomb like barrier-layer surface on the bottom of the AAO membrane [23, 24].

(2) *Modification of the porous nanopore surface and the barrier-layer surface*

Two types of surface modification of the AAO membrane were conducted to prepare two different nanostructured surfaces. First, the porous nanopore surface was immersed in a 35 wt% phosphoric acid at 28 °C for 18 min to modify the surface structure. The barrier-layer surface was processed for 10 min to achieve nano-hemispheres surface.

(3) *Deposition of silver thin film*

As shown in Figure 1(A), a three-dimensional (3D) nanostructured silver thin film was deposited onto the surface-modified porous nanopore surface and barrier-layer surface through radio frequency magnetron sputtering with the following conditions at room temperature: pressure = 4.0×10^{-3} torr, argon = 20 sccm, and power = 80 W.

3) *Packaging of the SERS chip*

The packaging process of the SERS substrate is shown in Figure 1(B). First, the silver film-sputtered AAO membrane was fixed on the glass slide, and a circular hole with a diameter of 2 mm was punched on the insulating tape. Then, the tape was pasted onto the AAO membrane to ensure the sensing area. Next, as shown in Figure 1(C), stock SNW solution (~2.5 OD) with a constant volume 5 µL was added at once and then dried. This step was repeated several times to pile up a nanowire disarray network. Thus, we obtained 5 µL × 1, 5 µL × 2···. 5 µL ×N of the SNW-deposited chip for drop casting and drying the analyte-containing aqueous solution, ready for subsequent SERS detection. As shown in Figure 1(C), the 5 µL × 3 SNW-deposited chip obtained the optimal performance.

B. Raman Spectroscopy

Raman micro-spectroscopy measurements were performed using the Micro Raman Identify Dual system (MRID-Raman, ProTrusTech Co., Ltd., Taiwan) mounted with one TE cooled CCD of 1024 × 256 pixels, as integrated by the manufacturer. To avoid laser-induced degradation, the system equipped with a 50× long working distance lens (Olympus America Inc., Center Valley, PA, USA) was operated at an excitation wavelength of 532 nm, with ~1 mW power.

The Raman spectra were recorded at a spectral resolution of 1 cm^{-1} in the spectral range between 400 and 2500 cm^{-1}. The exposure time for Raman spectra was 1 s, and each spectrum was accumulated at one time.

III. Results and Discussion

A. SNW Synthesis

In this study, PVP was used as an end-capping agent and a template to synthesize SNWs using the polyol method. Figure 2 shows the characteristics of the synthesized SNWs, which are all wrapped with PVP. As shown in Figure 2(A), the SNWs are staggered, with a length exceeding 20 µm, and an extremely high aspect ratio. As can be seen in the inset, each SNW has a width of about 80 nm, and its surface is wrapped by a 5 nm-thick PVP layer. The ultraviolet-visible (UV-Vis) absorption spectrum of the SNW solution is shown in Figure 2(B). As can be seen, the highest absorption peak is about 400 nm, with a wide absorption range from 320–700 nm. In addition, we also used the absorbance value of the highest absorption peak to define the concentration of the SNW solution. The SNW solution was diluted with water to the absorbance value of 1 (OD = 1).

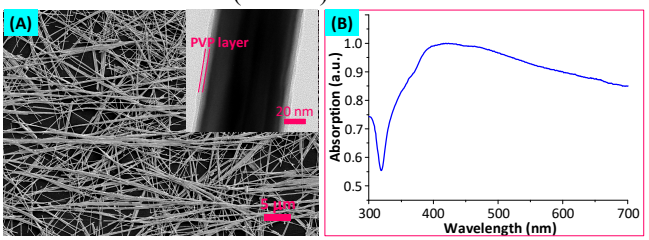

Fig 2. Characteristics of the synthesized SNWs. (A) SEM and TEM (inset) images; (B) Absorption spectrum

B. AAO Substrate Preparation

1) *Porous nanopore surface and the barrier-layer surface modification*

In this study, phosphoric acid was used to modify the porous nanopore surface and the barrier-layer surface of AAO, because phosphoric acid can isotropically etch AAO. Figure 3(A) shows the surface morphology of the AAO porous nanopore surface after being etched with phosphoric acid for 18 min. As the pores are arranged in a honeycomb shape, it can be seen that the thickness of the alumina wall at the three-cell joint is greater than the distance between two adjacent pores. By adjusting the phosphoric acid etching time, a nano tip can be created at the three-cell joint, thereby increasing the probability of hot spots being generated after sputtering the silver thin film. From Figure 3(B), it can also be observed that the AAO barrier-layer surface is closely arranged in a honeycomb pattern after being etched by phosphoric acid for 10 min. The diameter of the nano-hemisphere is about 100 nm, and a gap of about 20–30 nm can be found between the hemispheres. This 20–30 nm-wide gap is enough to prevent the subsequent nano silver sputtering from filling the gap and causing the surface to flatten. Moreover, this gap can be further utilized to increase the number of hot spots.

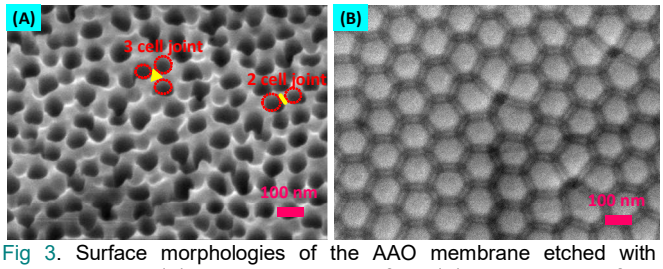

Fig 3. Surface morphologies of the AAO membrane etched with phosphoric acid. (A) porous nanopore surface; (B) barrier-layer surface

2) *Silver thin film deposition*

To enhance the surface plasma effect, a silver thin film was sputtered on the phosphoric acid-treated rough AAO porous nanopore surface and barrier-layer surface. The morphologies of the phosphoric acid-treated AAO porous nanopore surface under various time periods (50, 100, 150, and

200 s) of silver thin film sputtering are presented in Figure A1. The varying degrees of silver aggregation and deposition at the nano tips shown in Figure 3A form an array of tiny silver bumps. The spaces between these bumps decreased as the processing time increased. When the sputtering time reached 200 s, most of the nano silver bumps were closely connected (Figure A1(D)). Meanwhile, Figure A2 shows the morphologies of the phosphoric acid-treated AAO barrier-layer surface under various sputtering process time periods (20, 30, 40, and 50 s). The nano silver particles uniformly distributed on the surface of the hemispheric array are shown in Figure 3(B). The spaces between nano silver particles decreased with the increase of the sputtering time. Furthermore, an array of nano silver clusters was obtained when the sputtering time reached 50 s (Figure A2(D). As suggested by the results, for both the porous nanopore surface and nanopore hemisphere surface, nano silver particles can be uniformly arranged by sputtering. Furthermore, the distance between adjacent particles can be adjusted depending on the processing time.

C. Direct Bilirubin Raman Spectroscopy

Direct bilirubin is a tetrapyrrole compound (Tetrapyrrole). The direct bilirubin sample used in this study was artificially synthesized (Sigma, Taiwan) and can be regarded as the standard product of direct bilirubin. Its structure is shown in Figure 4(A). This kind of disodium salt is suitable as a direct bilirubin standard, which behaves in the same way as purified bilirubin glucuronides from human bile in diazo tests. The main characteristic peaks of the Raman spectrum of direct bilirubin powder are shown in Figure 4(B). As can be seen, the corresponding functional groups of the characteristic peaks are 687 cm^{-1} (C=O bond in the =COOH group), 962 cm^{-1} (C-H and C-H_3), 1,260 cm^{-1} (C-C and N-H_3 in the aromatic ring), 1,334 cm^{-1} (C-H_3 deformation and C-H in-plane bending), 1,457 cm^{-1} (C-C and C-N stretching), and 1,616 cm^{-1} (C-C in aromatic ring) [25]. Even though Raman spectrometer can measure the Raman spectrum of direct bilirubin powder, the intensity is still relatively low, thereby limiting the application of Raman spectroscopy in direct bilirubin detection.

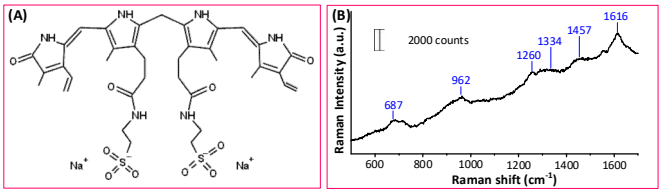

Fig 4. (A) Structure of direct bilirubin; (B) Raman spectrum of direct bilirubin powder

D. SERS Chip Optimization

The distributed densities of tiny silver nano bumps (Figure A1) or silver nano clusters (Figure A2) in the AAO substrate achieve the plasma field strength, as mentioned in Section 3B2), in which the smaller the gap, the stronger the hot spot strength. Furthermore, the packing density of SNWs on the AAO substrate is another main factor affecting the intensity of the SERS spectra. The intersection between SNWs can support the intrinsic hot spot; meanwhile, the contact between SNW and the tiny silver nanostructure on AAO may support the extra hot spot. The proposed SERS chip can offer three kinds of hot spots, thus producing local surface plasmon resonance in the gap of a metal nanostructure. The plasma enhancement of the SERS substrates determines the strength and density of the hot spots. In this study, SPR enhancing ability was optimized by adjusting the amount of SNW and the density of nano silver particles, as discussed below.

1) SNW SERS optimization

A SNW cluster possesses excellent SPR effect at high density and complex interlaced positions [22, 26]. Therefore, to enhance the intensity of the Raman spectrum, SNWs can be deposited onto the AAO substrate. Different volumes (5, 10, 15, 20, and 25 µL) of SNWs (with constant concentration) were respectively dropped into a circular detection zone with a diameter of 2 mm on the slide to form nano silver wire SERS substrates. The surface roughness levels of different SNW SERS substrates were then measured using an atomic force microscope. The morphologies and surface roughness of SNW SERS substrates of various volumes of SNW are shown in Figure A3. As can be seen, SERS substrates deposited with 15 µL SNWs produced the maximum surface roughness.

Furthermore, 10 µL of the direct bilirubin solution with a concentration of 10^{-5} M was dropped on each SNW SERS substrate, and the after which the Raman spectrum was measured after being left to air-dry. Figure 5(A) shows the measured Raman spectra. The peak values of direct bilirubin at 1616 cm^{-1} on different nano silver SERS substrates are shown in Figure 5(B). The substrate deposited with 15 µL of SNW has the highest roughness. Thus, it can generate the hot spot with the highest intensity and the best SERS enhancement effect.

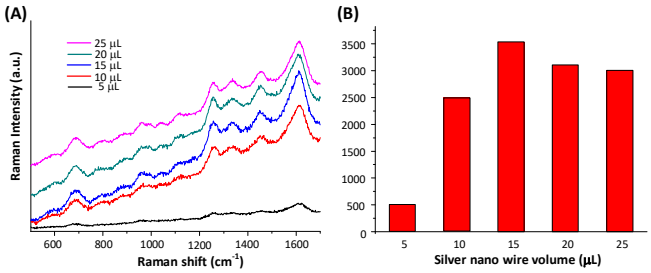

5. Raman spectra and Raman intensities of the direct bilirubin on different SNW SERS substrates. (A) Raman spectra; (B) Raman intensities at a peak value of 1,616 cm^{-1}

2) Composite SERS substrates

We first used porous nanopore SERS substrates and the corresponding SNW-coated SERS substrates to detect the direct bilirubin solution with a concentration of 10^{-5} M. Then, we examined the intensity at a peak value of 1,616 cm^{-1} to investigate the effect of different surface nanostructures on SERS. Figure 6 presents the Raman spectra and peak intensities at 1,616 cm^{-1} of the direct bilirubin on different SERS chips, which were sputtered with silver thin films under various processing times (50, 100, 150, and 200 s). Among the porous nanopore SERS substrates, the substrate that went through 150 s of silver sputtering produced the most intensive spectrum. Compared to the surface morphology shown in Figure A1(C), the suitable space between tiny silver bumps induced the maximum hot spot strength. Furthermore, the Raman spectra of the direct bilirubin were largely enhanced. The results indicated that the composite porous nanopore SERS substrates (SNW-coated porous nanopore SERS substrates) can achieve

the double SPR enhancing effect.

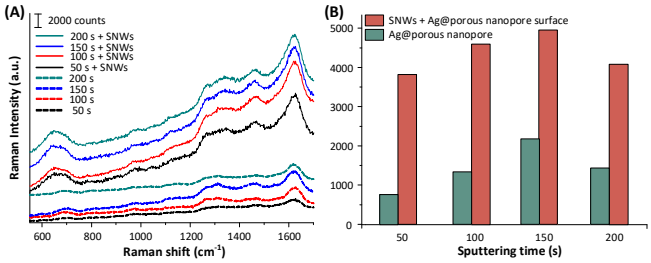

Fig 6. Raman spectra and Raman intensities of the direct bilirubin on different porous nanopore SERS substrates. (A) Raman spectra; (B) Raman intensities at a peak value of 1,616^{-1} cm

The nano-hemisphere AAO substrates and the corresponding SNW-coated SERS chips were further used to detect the direct bilirubin solution with the same concentration. The Raman spectra and Raman intensities at a peak of 1,616 cm^{-1} of the direct bilirubin on different SERS chips with variable nano-hemispheres (sputtering times of 20, 30, 40, and 50 s) of AAO substrates are shown in Figure 7. As can be seen, the substrate that went through 30 s of silver sputtering generated the most intensive spectrum due to the suitable space between the nano silver particles. Furthermore, the Raman spectra of the direct bilirubin were vastly enhanced. The results also indicated that the Raman spectra of the direct bilirubin were enhanced by the composite nano-hemisphere SERS chips (SNW-spread nano-hemisphere SERS substrates).

The above experiments indicate that both the composite porous nanopore and nano-hemisphere SERS substrates can vastly enhance the Raman spectrum intensity of the direct bilirubin. The nano-hemisphere SERS chip that went through 30 s of silver sputtering and was coated with 15 µL SNWs produced the strongest intensity among all the substrates. Therefore, this optimum composite SERS chip was used for further experiments to establish the calibration curve for direct bilirubin detection.

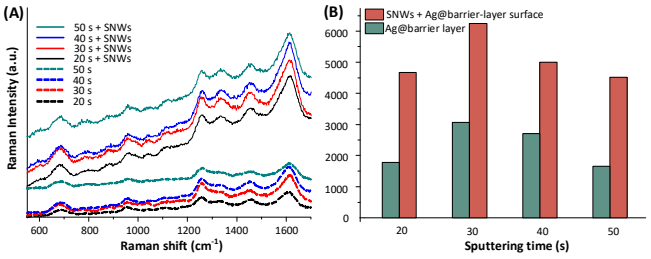

Fig 7. Raman spectra and Raman intensities of the direct bilirubin on different barrier-layer SERS substrates. (A) Raman spectra; (B) Raman intensities at a peak value of 1,616^{-1} cm

E. Calibration Curve for Direct Bilirubin Detection

Figure 8(A) illustrates the Raman spectra of direct bilirubin samples with various concentrations (10^{-4}, 10^{-5}, 5×10^{-6}, 10^{-6}, 10^{-7}, and 10^{-8} M) using the optimum composite SERS chip. The spectra of concentrations 10^{-8}–10^{-6} were magnified, as shown in the inset. As can be seen, the spectrum intensity increases with the increase of the direct bilirubin concentration. Given that the signal-to-noise rate (SNR) of the limit of detection of Raman spectroscopy must be at least three [27], the limit of detection of direct bilirubin was estimated to be around 10^{-7} M (SNR at 1,616 cm^{-1} = 3.37). Meanwhile, for direct bilirubin detection, the corresponding calibration curve of the Raman intensity at a peak value of 1,616 cm^{-1} is shown in Figure 8(B). The calibration curve can be used for a wide detection range from 10^{-7}–10^{-4} M, with R^2 = 0.98336. The concentrations of direct bilirubin samples in normal human serum range between 1.0–5.1 µM. Concentrations higher than 5.1 µM very likely indicate biliary atresia. Thus, the method proposed in this study can effectively detect direct bilirubin.

Furthermore, we measured the spectral 1,616 cm^{-1} peak intensity of direct bilirubin at 15 different locations on the substrate. The statistical relative standard deviation of the results was 4.6%, and the reproducibility (N = 3) was 2.2%. Both values indicated good reproducibility among different SERS substrates.

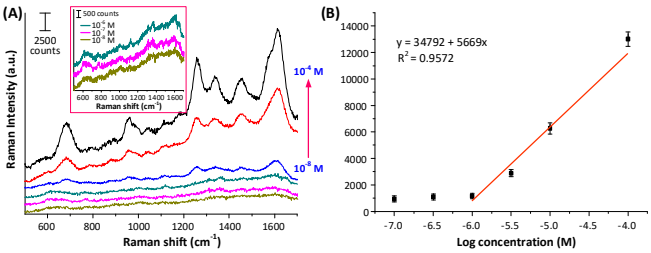

8. (A) Raman spectra of direct bilirubin using the optimum composite SERS substrates; (B) the corresponding calibration curve of Raman intensity at a peak value of 1,616^{-1} cm.

F. Performances Comparisons with the existing Bilirubin-Detection Systems

The performances comparisons of the proposed scheme with existing systems are listed in Table 1 below. Our system possesses advantages of low cost, high specificity, high sensitivity, and label free.

Tab 1. Performances comparisons with existing detection systems

Methods	Advantages	Disadvantage	Time	Ref.
HPLC	1. Non-interference with other heme protein 2. High Sensitivity	1. Instrument expensive 2. Need professional operate	> 20 min	[14]
Electrochemical detection	1. Detection limit to 0.1 nM 2. Detection range: 0.01-500 mM	1. Need enzyme 2. Expensive chip	> 20 min	[15]
Absorption spectrometry	simple and fast	1. Accuracy is not so high 2. Easily affected by carotenoids	< 5 min	[16]
Fluorometry	1. simple and fast 2. enzyme-free	Susceptible to environmental factors (pH, temperature)	< 5 min	[19]
SERS	High specificity, sensitivity label-free	Complicated chip preparation (high cost)	< 5 min	[21]
This work	Low cost, high specificity, sensitivity, label-free	Required a Raman spectroscopy	< 5 min	

IV. Conclusion

Biliary atresia, a known congenital disease, is the most common cause of childhood liver disease and the main cause of liver replacement. As explained earlier, the development of early screening and early diagnosis technology can effectively improve the therapeutic effect on children with biliary atresia. Thus, in this study, a novel approach for detecting direct bilirubin by Raman spectroscopy is proposed. The main feature

of this method is that it uses composite SERS chips, which we created by coating SNW on the surface of an AAO membrane. Both the nano-hemisphere and porous nanopore surfaces of an AAO membrane were used as the AAO substrate. The Raman intensity at a peak value of 1,616 cm^{-1} was used as the index for direct bilirubin detection. Experimental results demonstrated that a broad detection range from 10^{-7}–10^{-4} M with R^2 = 0.98336 was achieved using only 10 µL of direct bilirubin. Furthermore, the detection limit of direct bilirubin detection was vastly improved by the double SPR enhancing effect of the composite SERS chip. Given that the concentration of direct bilirubin in normal human serum is within 1.0–5.1 µM, the method proposed in this study can thus effectively detect direct bilirubin.

APPENDIX

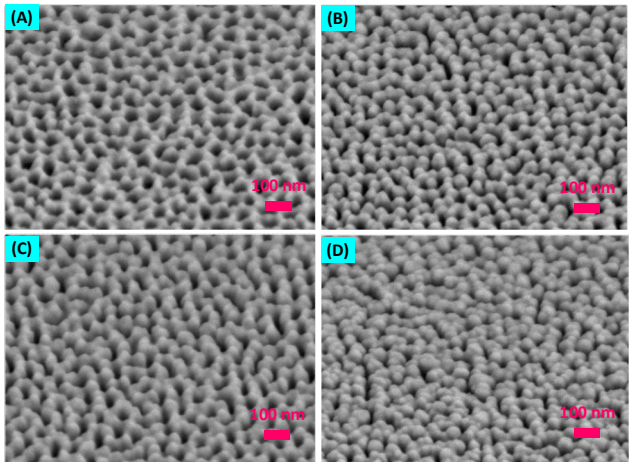

Fig A1. Morphologies of the phosphoric acid treated AAO porous nanopore surface under various process times of silver sputtering. (A) 50 s;(B)100 s;(C) 150 s;(D) 200 s

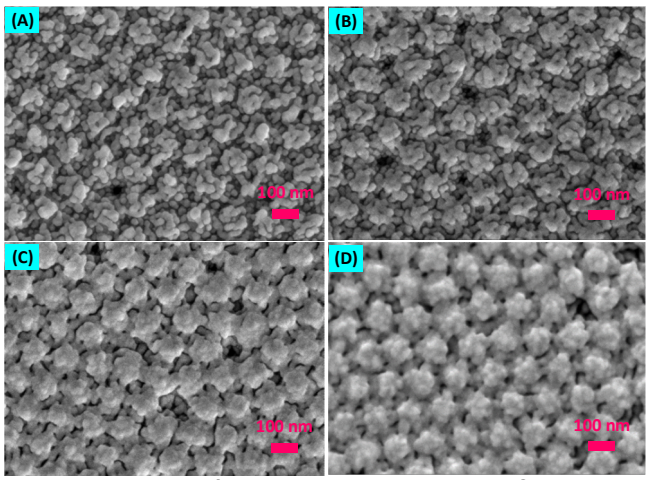

Fig A2. Morphologies of the phosphoric acid treated AAO barrier-layer surface under various process times of silver sputtering. (A) 20 s;(B)30 s;(C) 40 s;(D) 50 s

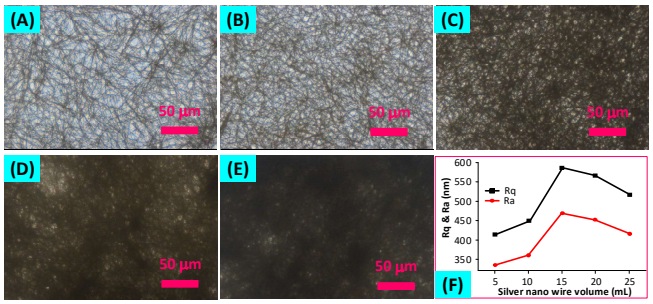

Fig A3. Morphologies and surface roughness of SNW SERS substrates. SNW concentration (A)5 µL; (B)10 µL; (C)15 µL; (D)20 µL; (E)25 µL; (F)surface roughness of substrates

ACKNOWLEDGMENT

The authors would like to offer their thanks to the Ministry of Science and Technology of Taiwan (grant # MOST-108-2622-E-005-017-CC2) for their financial support of this research. The authors also thank the ProTrusTech Co., Taiwan for providing the Raman spectroscopy.

REFERENCES

[1] J. L. Hartley, M. Davenport, and D. A. Kelly, "Biliary atresia," *The Lancet,* vol. 374, pp. 1704-1713, 2009.

[2] D. M. Hays and W. H. Snyder, "Life-span in untreated biliary atresia," *Surgery,* vol. 54, pp. 373-375, 1963.

[3] Y.-H. Gu, K. Yokoyama, K. Mizuta, T. Tsuchioka, T. Kudo, H. Sasaki, *et al.*, "Stool Color Card Screening for Early Detection of Biliary Atresia and Long-Term Native Liver Survival: A 19-Year Cohort Study in Japan," *The Journal of Pediatrics,* vol. 166, pp. 897-902.e1, 2015.

[4] M.-O. Serinet, B. E. Wildhaber, P. Broue, A. Lachaux, J. Sarles, E. Jacquemin, *et al.*, "Impact of age at Kasai operation on its results in late childhood and adolescence: a rational basis for biliary atresia screening," *Pediatrics,* vol. 123, pp. 1280-1286, 2009.

[5] S. Harpavat, M. J. Finegold, and S. J. Karpen, "Patients with biliary atresia have elevated direct/conjugated bilirubin levels shortly after birth," *Pediatrics,* vol. 128, pp. e1428-e1433, 2011.

[6] C. Tiribelli and J. D. Ostrow, "The molecular basis of bilirubin encephalopathy and toxicity: Report of an EASL Single Topic Conference, Trieste, Italy, 1-2 October, 2004," *Journal of Hepatology,* vol. 43, pp. 156-166, 2005.

[7] R. Bonnett, J. E. Davies, and M. B. Hursthouse, "Structure of bilirubin," *Nature,* vol. 262, pp. 326-328, 1976.

[8] T. D. Boyer and D. Zakim, *Hepatology: a textbook of liver disease*: Saunders, 1990.

[9] X. Wang, J. R. Chowdhury, and N. R. Chowdhury, "Bilirubin metabolism: Applied physiology," *Current Paediatrics,* vol. 16, pp. 70-74, 2006.

[10] D. G. Levitt and M. D. Levitt, "Quantitative assessment of the multiple processes responsible for bilirubin homeostasis in health and disease," Clinical and experimental gastroenterology, vol. 7, p. 307, 2014.

[11] L. Ngashangva, V. Bachu, and P. Goswami, "Development of new methods for determination of bilirubin," Journal of Pharmaceutical and Biomedical Analysis, vol. 162, pp. 272-285, 2019.

[12] R. Rawal, P. R. Kharangarh, S. Dawra, M. Tomar, V. Gupta, and C. S. Pundir, "A comprehensive review of bilirubin determination methods with special emphasis on biosensors," Process Biochemistry, vol. 89, pp. 165-174, 2020.

[13] W. Tan, L. Zhang, J. C. G. Doery, and W. Shen, "Study of paper-based assaying system for diagnosis of total serum bilirubin by colorimetric diazotization method," Sensors and Actuators B: Chemical, vol. 305, p. 127448, 2020.

[14] V. K. Bhutani, L. H. Johnson, and G. Gourley, "Measuring bilirubin through the skin?," Pediatrics, vol. 111, pp. 919-920, 2003.

[15] N. Chauhan, R. Rawal, V. Hooda, and U. Jain, "Electrochemical biosensor with graphene oxide nanoparticles and polypyrrole interface for the detection of bilirubin," Rsc Advances, vol. 6, pp. 63624-63633, 2016.

[16] S. C. Kazmierczak, A. F. Robertson, P. G. Catrou, K. P. Briley, B. L. Kreamer, and G. R. Gourley, "Direct spectrophotometric method for

measurement of bilirubin in newborns: comparison with HPLC and an automated diazo method," Clinical chemistry, vol. 48, pp. 1096-1097, 2002.
[17] Y. Andreu, J. Galbán, S. de Marcos, and J. R. Castillo, "Determination of direct-bilirubin by a fluorimetric-enzymatic method based on bilirubin oxidase," Fresenius' journal of analytical chemistry, vol. 368, pp. 516-521, 2000.
[18] Y. Andreu, M. Ostra, C. Ubide, J. Galbán, S. de Marcos, and J. R. Castillo, "Study of a fluorometric-enzymatic method for bilirubin based on chemically modified bilirubin-oxidase and multivariate calibration," Talanta, vol. 57, pp. 343-353, 2002.
[19] M. Santhosh, S. R. Chinnadayyala, A. Kakoti, and P. Goswami, "Selective and sensitive detection of free bilirubin in blood serum using human serum albumin stabilized gold nanoclusters as fluorometric and colorimetric probe," Biosensors and Bioelectronics, vol. 59, pp. 370-376, 2014.
[20] B. Shan, Y. Pu, Y. Chen, M. Liao, and M. Li, "Novel SERS labels: Rational design, functional integration and biomedical applications," Coordination Chemistry Reviews, vol. 371, pp. 11-37, 2018.
[21] X. Pan, L. Li, H. Lin, J. Tan, H. Wang, M. Liao, et al., "A graphene oxide-gold nanostar hybrid based-paper biosensor for label-free SERS detection of serum bilirubin for diagnosis of jaundice," Biosensors and Bioelectronics, vol. 145, p. 111713, 2019.
[22] C. T. Huang, F. J. Jan, and C. C. Chang, “A 3D Plasmonic Crossed-Wire Nanostructure for Surface-Enhanced Raman Scattering and Plasmon-Enhanced Fluorescence Detection”, *Molecules*, vol. 26, pp. 281, 2021.
[23] J. J. Tsai, I. J. Bau, H. T. Chen, Y. T. Lin, G. J. Wang, “A Novel Nanostructured Biosensor for the Detection of the Dust Mite Antigen Der p2”. *International Journal of Nanomedicine*, vol. 6, pp. 1201-1208, 2016.
[24] Y. T. Tung, C. C. Chang, Y. L. Lin, S. L. Hsieh, and G. J. Wang, Development of double-generation gold nanoparticle chip-based dengue virus detection system combining fluorescence turn-on probes. *Biosensors and Bioelectronics,* vol.77, pp. 90–98, 2016.
[25] F. Celis, M. Campos-Vallette, J. Gómez-Jeria, R. Clavijo, G. Jara, and C. Garrido, "Surface-enhanced Raman scattering and theoretical study of the bilichromes biliverdin and bilirubin," *Spectroscopy Letters*, vol. 49, pp. 336-342, 2016.
[26] J.W. Jeong, M.M. Arnob, K.M. Baek, S.Y. Lee, W.C. Shih, and Y.S. Jung, “3D Cross-Point Plasmonic Nanoarchitectures Containing Dense and Regular Hot Spots for Surface-Enhanced Raman Spectroscopy Analysis”, *Advance Materials*, vol. 28, pp. 8695-8704, 2016.
[27] L. K. Lim, B. K. Ng, C. Y. Fu, L. Y. M. Tobing, and D. H. Zhang, "Highly sensitive and scalable AAO-based nano-fibre SERS substrate for sensing application," *Nanotechnology,* vol. 28, 235302, 2017.